

OPEN ACCESS

Modal solutions for SH guided waves radiated by an EMAT in a ferromagnetic plate

To cite this article: C Rouge *et al* 2012 *J. Phys.: Conf. Ser.* **353** 012014

View the [article online](#) for updates and enhancements.

You may also like

- [Reconstructing echoes completely submerged in background noise by a stacked denoising autoencoder method for low-power EMAT testing](#)
Jinjie Zhou, Dianrui Yu, Xiang Li et al.
- [Magnetic phase transitions in \$Gd_{64}Sc_{36}\$ studied using non-contact ultrasonics](#)
Oksana Trushkevych, Yichao Fan, Robert Perry et al.
- [Electromagnetic acoustic transducer for receiving longitudinal wave in the central hole of the wind turbine main shaft](#)
Jun Cheng, Yan Lyu, Hao Chen et al.



ECS
The
Electrochemical
Society
Advancing solid state &
electrochemical science & technology

DISCOVER
how sustainability
intersects with
electrochemistry & solid
state science research

Modal solutions for SH guided waves radiated by an EMAT in a ferromagnetic plate

C Rouge, A Lhémercy and D Ségur

CEA, LIST, F-91191 Gif-sur-Yvette, France

E.mail: alain.lhemery@cea.fr

Abstract. Electromagnetic acoustic transducers (EMAT) generate forces which are sources of elastic waves in a part without contact with it. Depending on the EMAT design, normal or tangential forces can be generated. Thanks to these capabilities, EMATs constitute an interesting alternative to piezoelectric devices in many configurations of non-destructive examination. In this paper, only shear horizontal (SH) guided waves radiated by an EMAT in a plate made of ferromagnetic material are modelled. These waves are particularly interesting to use for testing welded structures: SH waves may propagate in a weld without scattering and mode conversion phenomena. All the forces generated by an EMAT (Lorentz's, magnetostrictive and magnetic forces) being exponentially decreasing with depth, they are rewritten as series of moments, then, approximated as equivalent surface stresses. Surface stresses are then taken into account as terms of source of elastic waves. Specific features of EMAT can eventually be exploited to derive simple analytic expressions of the applied stress, leading to closed-form solutions for the modal amplitude of SH guided waves. Using these solutions, which are calculated at no computing cost, it becomes easy to study the influence of typical EMAT parameters on the modal amplitude of waves generated in the plate.

1. Introduction

Guided waves are used in NonDestructive Testing because they can propagate over long distance. They are often generated by piezoelectric transducers, but they can also be generated by Electro-Magnetic Acoustic Transducers (EMAT). Many designs of EMAT were experimentally studied and the ultrasound generation is well-known in a non-ferromagnetic metal [1]. The current in the EMAT induces currents in the part under test, known as eddy currents, which, with the superposed bias magnetization, create a force, the Lorentz force, confined in the vicinity of the part surface. In a ferromagnetic medium, EMATs create two more forces, also confined near the surface: the magnetization force and the magnetostriction force. Many EMAT designs have been studied to generate various kinds of elastic wave fields of various polarizations; for example, SH guided waves are more easily generated by means of specific EMAT design than with piezoelectric transducers. Besides, the fact that there is no contact of the EMAT with the part under test allows high speed inspection. EMATs can also work in hostile conditions such as high temperature or high pressure environments. However, those benefits are counteracted by the fact that EMAT signals are generally of much lower amplitude than that generated by piezoelectric transducers.

In weld inspection, SH waves have a specific interest because typical inner structure of welds may appear as a homogeneous material for them (figure 1) if the heterogeneous and anisotropic structure is bi-dimensional and the wave polarization is normal to it. The aim of the present paper is to develop a

model for predicting the radiation of SH guided waves in a ferromagnetic plate-like structure by EMATs; such a model is helpful for optimizing the design of EMAT to get higher signal amplitude.

This work is based on modal description of guided waves to ease the interpretation of typical complex waveforms in guided wave inspection; one can further assume that similarly, the interpretation in terms of guided modes of the field radiated in a rather complex way by an EMAT in ferromagnetic materials shall also be made easier. Under a modal description of fields, the particle velocity and stress fields, solutions of the elastodynamic field equations governing the propagation of elastic waves, are expressed as linear combinations of the modes likely to exist. The part geometry considered herein is that of a plate made of homogeneous and isotropic ferromagnetic metal (iron, nickel). To simplify the problem, the analysis is made in 2D as shown on figure 1. As far as SH guided waves for weld inspections are concerned, this simplification makes sense since their specific interest only holds if the 2D symmetry reasonably applies.

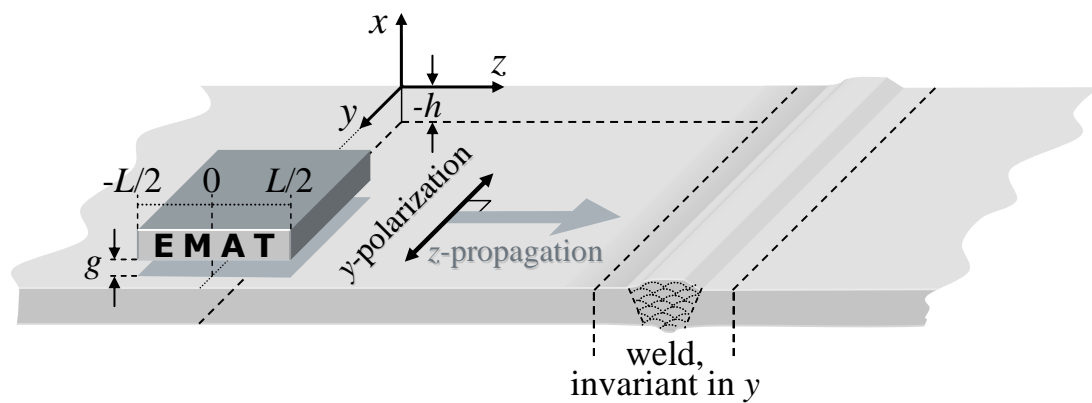


Figure 1. 3D representation of the configuration of the plate and the EMAT studied.

The present paper is organized as follows. In a first part, the theoretical model of SH wave radiation in ferromagnetic materials by EMATs is derived: closed-form solutions for the magnetic excitation field and the body forces it creates are derived; body forces are converted into surface stress sources of an elastodynamic problem solved as a modal series. In a second part, examples of application of our model illustrate some of the model capabilities.

2. Theory

The present paragraph is dedicated to the derivation of the global model for predicting SH guided waves radiated by an EMAT in a ferromagnetic plate. It is made of a succession of semi-analytical solutions of sub-problems. Semi-analytical solutions indeed can be easily translated into simulation tools allowing efficient computation works for optimizing NDT configurations.

At first, a closed-form solution for the magnetic field created by an EMAT is given by accounting for the periodicity of typical wire arrangement in classical EMAT designs. Then, body forces generated in a ferromagnetic plate are described as functions of the magnetic field. These forces are then transformed as equivalent surface stresses, for they are confined close to the surface where the magnetic field applies. A generic formula for the Green's function describing SH modes generated by a surface stress in a plate is then proposed. This last formula is eventually used in a convolution integral to predict modal amplitudes of SH guided waves generated by EMATs.

2.1. Magnetic field created by an EMAT

The magnetic field in the material can be deduced from Maxwell's equations and Ohm's law under the following assumptions:

- all quantities vary harmonically with time so that a term $\exp(i\omega t)$ can be factorized in the various equations, ω being the pulsation [$\text{rad}\cdot\text{s}^{-1}$] and t is the time [s];

- time-dependency of current displacement in Maxwell-Ampere's law is neglected because, at typical EMAT working frequencies, current displacement can be considered as permanent compared to particle displacement;
- magnetostriction causes no volume change. This is true for isotropic ferromagnetic metal.

The first assumption allows the Maxwell-Faraday and Maxwell-Ampere equations to be written as:

$$\vec{\nabla} \wedge \vec{E} = -\frac{\partial \vec{B}}{\partial t}, \quad (1a)$$

$$\vec{\nabla} \wedge \vec{H} = \vec{J}. \quad (1b)$$

Besides, the relations between the magnetic field \vec{B} [T], the magnetic excitation field \vec{H} [A.m⁻¹] and the magnetization field \vec{M} [A.m⁻¹] are:

$$\vec{B} = \mu_0(\vec{H} + \vec{M}), \quad (2a)$$

$$\vec{M} = \chi \vec{H}, \quad (2b)$$

$$\vec{B} = \mu_0 \mu \vec{H}, \quad (2c)$$

where μ_0 is the vacuum permeability ($=4\pi \times 10^{-7}$ H.m⁻¹), μ is the magnetic permeability and χ the magnetic susceptibility. Here, for sake of simplicity, we further assume that magnetic permeability of the material μ is constant; this assumption is verified as long as \vec{B} linearly varies with \vec{H} . It shall otherwise be accounted for as a matrix [1] whose components vary with both the frequency and the amplitude of the magnetic field [2, 3].

From now on, we assume that the current flows in the coil along the y -axis. With the help of Ohm's law and under the few assumptions made, the magnetic excitation field is a solution of the following system of equations:

$$\frac{\partial H_x}{\partial x} = -\frac{\partial H_z}{\partial z}, \quad (3a)$$

$$H_y = 0, \quad (3b)$$

$$\left(\frac{\partial^2}{\partial x^2} + \frac{\partial^2}{\partial z^2} \right) H_z - j\omega\sigma\mu_0\mu H_z = 0. \quad (3c)$$

The current in the electric circuit is now written as a Fourier series (as done in [4, 5]). The current distribution can be described as a sequence of 0, 1 and -1 values along the z -axis. This Fourier series is denoted by $S(z)$ and is given by:

$$S(z) = \sum_{n=0}^{\infty} S_n(z) = \sum_{n=0}^{\infty} \left[S_n^c \cos(s_n z) + S_n^s \sin(s_n z) \right]. \quad (4)$$

The integral formulation of Maxwell-Ampere law is used to write boundary conditions of equation (3c) just below the electric circuit of the EMAT, at $x = g$ where g [m] is the lift-off. One gets:

$$H_z^A(g, z) = \frac{I}{2a} S(z), \quad (5)$$

where I denotes the current intensity [A] and a , the wire width [m]. Superscript "A" stands for quantities defined in air. With this boundary condition, equation (3c) for magnetic field is solved in the volume between the coil and the plate. One gets

$$H_z^A(x, z) = \frac{I}{2a} \sum_{n=0}^{\infty} S_n(z) \exp s_n(g-x) \quad \text{for } x \in [0, g] . \quad (6)$$

The solution for \vec{H} in the plate is then obtained by solving equation (3c) by taking into account the continuity of tangential field at the interface between air and the plate. After simple algebra, the elementary solution of this differential equation is obtained as:

$$H_x(x, z) = \frac{I}{2a} \sum_{n=0}^{\infty} \frac{s_n}{q_n} S_n(z) \exp(-s_n g) \exp(q_n x), \quad H_z(x, z) = \frac{I}{2a} \sum_{n=0}^{\infty} S_n(z) \exp(-s_n g) \exp(q_n x) \quad (7)$$

with $q_n = s_n^2 + 2j / \delta^2$ and $\delta = 2 / \omega \sigma \mu_0 \mu^{1/2}$.

This is a separate variable solution in x and z . Its z -dependency is a function of the coil geometry only, through the Fourier series $S(z)$. Its x -dependency is a decreasing exponential with depth that is a function of coil parameters and material characteristics through the penetration depth δ [m].

2.2. Body forces generated by a magnetic field into a ferromagnetic medium

As mentioned in the introduction, considering a plate made of a ferromagnetic material makes it necessary to account for two more forces than the sole Lorentz's forces an EMAT creates in non-ferromagnetic one. The three forces to consider generated by the magnetic field imposed by the EMAT are thus the Lorentz's force plus the magnetization and the magnetostriction forces. The present paragraph aims at expressing them.

2.2.1. Lorentz's force. The Lorentz's force results from the interaction of the eddy current density $\vec{J}_e = \vec{\nabla} \wedge \vec{H}$ created by the coil with the total magnetic field; the total magnetic field is the sum of the static magnetic field \vec{B}_0 of the magnet and the dynamic magnetic field $\mu_0 \mu \vec{H}$, as calculated in the previous paragraph. The force is expressed by:

$$\vec{F}_L = (\vec{\nabla} \wedge \vec{H}) \wedge (\vec{B}_0 + \mu_0 \mu \vec{H}) . \quad (8)$$

2.2.2. Magnetization force. The interaction between the dynamic magnetic field \vec{H} and the magnetization vector of the magnet \vec{M}_0 and that of the metal \vec{M} induces the reorientation of magnetic dipoles in the metal. This results in the so-called magnetization force, expressed by:

$$\vec{F}_M = \mu_0 \mu (\vec{\nabla} \vec{H}) \times (\vec{M} + \vec{M}_0) . \quad (9)$$

2.2.3. Magnetostriction force. This force is generated by deformation of magnetic domains due to the interaction between the dynamic magnetic field and the static magnetic field. It is classically compared to piezoelectricity and often called "piezomagnetic" effect. The (6x3) tensor \vec{e} of piezomagnetic stress coefficients is introduced to derive the magnetostriction stress tensor as

$$\sigma_{MS}^I = -e_{Ij} H_j , \quad \text{with } I \in \{1, \dots, 6\} , \quad (10)$$

from which the magnetostriction force is readily obtained. The force is given by:

$$\begin{aligned}
\vec{F}_{MS}^x &= \frac{\partial \sigma_{MS}^1}{\partial x} + \frac{\partial \sigma_{MS}^6}{\partial y} + \frac{\partial \sigma_{MS}^5}{\partial z}, \\
\vec{F}_{MS}^y &= \frac{\partial \sigma_{MS}^6}{\partial x} + \frac{\partial \sigma_{MS}^2}{\partial y} + \frac{\partial \sigma_{MS}^4}{\partial z}, \\
\vec{F}_{MS}^z &= \frac{\partial \sigma_{MS}^5}{\partial x} + \frac{\partial \sigma_{MS}^4}{\partial y} + \frac{\partial \sigma_{MS}^3}{\partial z}.
\end{aligned} \tag{11}$$

In a more condensed form, one writes:

$$\vec{F}_{MS} = -\vec{\nabla}'(\bar{e}\vec{H}), \tag{12}$$

where the notation $\vec{\nabla}'$ denotes a modified gradient as written by Auld [6].

Note that \bar{e} itself depends on the total magnetic field, sum of the static and dynamic terms as mentioned previously. The former term is of higher amplitude than the latter. As a consequence, we consider here that dynamic effects are negligible, as far as the evaluation of \bar{e} is concerned. However, variations of \bar{e} as a function of the amplitude of the static field result from quite complex microphysics phenomena. Readers interested in a detailed discussion about the possible variations of \bar{e} are referred to [7]. In what follows, we consider that the various components of \bar{e} involved in the calculation of the magnetostriction force are constant values. As a consequence, doubling frequency effect sometimes described in the literature [8, 9] cannot be accounted for.

2.3. Transformation of body forces into equivalent surface stresses

The three body forces created by the EMAT could be straightforwardly integrated to predict the elastic wave field they generate, in the form of a triple (volume) convolution integral of the forces with the elastodynamic Green's function for the problem in hand. However, since they were all expressed as functions of the magnetic field calculated in paragraph 2.1., they also exponentially decrease with depth, with a decreasing factor δ (penetration depth).

To avoid integrating forces onto a volume, Thompson [10] developed an approximate modelling approach to transform the volume integral over forces onto a surface integral over equivalent surface stress. The approximation used, which we re-develop in what follows, is all the more accurate since forces are confined in the vicinity of the surface where the EMAT is used.

The elastic wave equation to be solved is given by the following equation where the right-hand side is the sum of the various forces described above. We have:

$$-\mu_L \Delta \vec{u} - (\lambda_L + \mu_L) \vec{\nabla}(\nabla \cdot \vec{u}) + \rho \frac{\partial^2 \vec{u}}{\partial t^2} = \vec{F}_L + \vec{F}_M + \vec{F}_{MS}, \tag{13}$$

where \vec{u} is the particle displacement [m], ρ the material density [$\text{kg}\cdot\text{m}^{-3}$] and λ_L and μ_L , the Lamé's constants [Pa] from Lamé's equation for an isotropic material.

From now on, we restrict our study to the generation of SH waves, propagating in the (x, z) plane polarized in the y -direction. Therefore, the problem in hand is bi-dimensional and we only have to predict the y -component of the particle displacement generated by forces applied in the y -direction. This restriction, which may seem severe at first glance, corresponds to actual symmetry of testing configurations of interest, in particular, for weld inspections (see figure 1); moreover, it leads to interesting simplifications in subsequent calculations. Note that the overall approach can be extended to the case of Lamb wave generation where forces to be considered apply along \vec{x} or \vec{z} direction and the wave particle polarization belongs to the (x, z) propagation plane.

Since the problem is 2D, the general triple integral over body force sources is restricted to a double integral in the (x, z) plane. Under the above assumptions, the SH wave displacement at an observation point \vec{r} can be written in the form of the following convolution Green's integral as:

$$u_y(\vec{r}) = \int_{-L/2}^{L/2} \int_{-\infty}^0 G_{yy}(\vec{r}, \vec{r}_0) f_y(\vec{r}_0) dx_0 dz_0, \quad (14)$$

limited along \vec{z} by the size L of the EMAT, and where G_{yy} denotes the only involved component of the Green's tensor thanks to the 2D / SH symmetry considered here. The source term reduces to

$$f_y(\vec{r}_0) = \left[(F_L + F_M + F_{MS}) \cdot \vec{e}_y \right] = - \left[e_{6x} \frac{\partial H_x}{\partial x_0} + e_{6z} \frac{\partial H_z}{\partial x_0} + e_{4x} \frac{\partial H_x}{\partial z_0} + e_{4z} \frac{\partial H_z}{\partial z_0} \right], \quad (15)$$

where only magnetostriction actually contributes, other forces being oriented in the (x, z) plane.

The detailed derivation for transforming body force convolution integral into a surface stress convolution integral is given in Appendix. It allows us to re-write equation (14) as:

$$u_y(\vec{r}) \approx \int_{-L/2}^{L/2} \left[T_y - \frac{1}{2} N_y \left(\frac{\omega^2 \rho}{C_{44}} + \frac{\partial^2}{\partial z_0^2} \right) \right] G_{yy}(\vec{r}, \vec{R}_0) dz_0, \quad (16)$$

where $\vec{R}_0 = \vec{r}_0(0, z_0)$, T_y and N_y defined in the Appendix are respectively the zeroth and the second order moments of body force f_y .

2.4. Green's function for SH waves generated in a plate by a surface stress

In equation (16), the Green's function, not explicitly given, stands for the elastodynamic solution of the problem of an elementary source at the surface of an elastic half-space. For solving the radiation in a plate, it is more convenient to make use of a more adapted Green's function that accounts for the finite thickness of the plate. More specifically, we want to derive such a function as a modal series of SH guided waves. This is done in the present subsection by using the integration over the plate thickness of the complex reciprocity relation [6].

Assuming a line source (along y) acting at (x_0, z_0) , the reciprocity relation described in [6] leads to the following formal relation

$$4 \frac{\partial}{\partial z} \sum_n A_n^{G_{yy}}(z, z_0) e^{j\beta_m^* z} P_{mn} + \left[\vec{v}_m^* \vec{\sigma}_n e^{j\beta_m^* z} + \vec{v}_n \vec{\sigma}_m^* e^{j\beta_m^* z} \right] \cdot \vec{e}_x \Big|_{x=-h}^{x=0} = 0, \quad (17)$$

where amplitudes of the n modes are obtained as solutions for the line source as

$$\vec{v}(x, z) = \sum_n A_n^{G_{yy}}(z) \vec{v}_n(x), \quad \vec{\sigma}(x, z) = \sum_n A_n^{G_{yy}}(z) \vec{\sigma}_n(x), \quad (18)$$

and where the state "m" is an arbitrary propagative mode:

$$\vec{v}_m(x, z) = \vec{v}_m(x) e^{-j\beta_m z}, \quad \vec{\sigma}_m(x, z) = \vec{\sigma}_m(x) e^{-j\beta_m z}. \quad (19)$$

The factor P_{mn} arises from the complex orthogonality relation and is given by [6, 11]:

$$P_{mn} = -\frac{1}{4} \int_{-h}^0 (\vec{v}_n^* \vec{\sigma}_m + \vec{v}_m \vec{\sigma}_n^*) \cdot \vec{z} dx. \quad (20)$$

The symbol * stands for conjugate complex values. Besides, the boundary conditions and the initial conditions are:

$$\vec{\sigma}_m(x=0, z) \cdot \vec{e}_x = \vec{\sigma}_m(x=-h, z) \cdot \vec{e}_x = 0, \quad \vec{\sigma}_n(x=-h, z) = \vec{0}, \quad \vec{\sigma}_n(x=0, z) = - \begin{pmatrix} 0 & 1 & 0 \\ 1 & 0 & 0 \\ 0 & 0 & 0 \end{pmatrix} \delta(z - z_0), \quad (21)$$

where h is the plate thickness and δ the Dirac function. Equation (17) becomes:

$$4 \sum_n A_n^{G_{yy}}(z, z_0) j \beta_m^* e^{j \beta_m^* z} P_{mm} + 4 \sum_n \frac{\partial A_n^{G_{yy}}(z, z_0)}{\partial z} e^{j \beta_m^* z} P_{mm} = \tilde{v}_{y_m}^*(x=0) e^{j \beta_m^* z} \delta(z - z_0), \quad (22)$$

where $\tilde{v}_{y_m}^*(x=0)$ is the amplitude of the particle velocity along the y -direction for the “ m mode” evaluated at the top surface of the plate and z is the distance between the line-source and the observation point.

Here, only real propagative modes are studied, inhomogeneous and evanescent modes vanishing far from the source. Therefore, conjugate complex values are equal to the real ones. Orthogonality relation implies “ $m = n$ ” [6]. Thus, modal amplitudes verify the following first order differential equation:

$$4P_{mm} \left(\frac{\partial}{\partial z} + j\beta_m \right) A_m^{G_{yy}}(z, z_0) = \tilde{v}_{y_m}^*(x=0) \delta(z - z_0), \quad (23)$$

which is easily solved as:

$$A_m^{G_{yy}}(z, z_0) = \frac{e^{-j\beta_m z}}{4P_{mm}} \tilde{v}_{y_m}^*(x=0) \int_{-\infty}^{+\infty} e^{j\beta_m \eta} \delta(\eta - z_0) d\eta = \frac{e^{-j\beta_m z}}{4P_{mm}} \tilde{v}_{y_m}^*(x=0) e^{j\beta_m z_0}. \quad (24)$$

This modal amplitude is that of the m -th propagative SH mode in a waveguide excited by a line source of tangential stress. Their wavenumber β_n is given analytically by:

$$\beta_n = \left(\frac{\rho \omega^2}{\mu_L} - \left(\frac{n}{h} \right)^2 \right)^{1/2}. \quad (25)$$

2.5. Modal amplitude of SH guided modes generated by an EMAT

Thanks to the modal decomposition, the displacement \tilde{u}_G generated by a tangential stress line source in the plate is now written as:

$$\tilde{u}_G(x, z, [z_0]) = \sum_m A_m^{G_{yy}}(z, z_0) \tilde{u}_m(x) = \sum_m \frac{e^{-j\beta_m z}}{4P_{mm}} \tilde{v}_{y_m}^*(x=0) e^{j\beta_m z_0} \tilde{u}_m(x). \quad (26)$$

This solution is now used for predicting the field radiated by forces created by an EMAT. Body forces have been transformed into equivalent surface stress that can be extracted from equation (16) in the form of an operator as

$$\sigma_{eq}(z_0) = \left[T_y - \frac{1}{2} N_y \left(\frac{\omega^2 \rho}{C_{44}} + \frac{\partial^2}{\partial z_0^2} \right) \right]. \quad (27)$$

Equation (16) was derived in the Green’s function convolution integral formalism assuming the Green’s function shall verify free boundary condition at $x = 0$ (half-space solution). The Green’s function derived in the previous subsection as a modal series also verifies the same boundary condition plus a similar condition at the boundary $x = -h$. At this surface, sources of body force may be considered as not contributing; this is true while $h \gg \delta$, a relation which is almost always verified for typical frequencies and materials of interest in NDT applications. Therefore, Green’s function for the elastic plate can be substituted for the original half-space solution in equation (16). By doing so, equation (16) straightforwardly becomes the solution for SH guided waves since the new kernel was built to account for the guided propagation. The particle displacement radiated at (x, z) by an EMAT is then found after rather simple algebraic calculations that follow:

$$\begin{aligned}
u_y(x, z) &= \int_{-L/2}^{L/2} \sigma_{eq}(z_0) G_{yy}(x, z, [z_0]) dz_0 = \int_{-L/2}^{L/2} \sigma_{eq}(z_0) \tilde{u}_G(x, z, [z_0]) dz_0 \\
&= \sum_m \tilde{u}_m(x) \frac{e^{-j\beta_m z}}{4P_{mm}} \tilde{v}_{y_m}(x=0) \int_{-L/2}^{L/2} \left[T_y - \frac{1}{2} N_y \left(\frac{\omega^2 \rho}{C_{44}} + \frac{\partial^2}{\partial z_0^2} \right) \right] e^{j\beta_m z_0} dz_0 \\
&= \sum_m \tilde{u}_m(x) \frac{e^{-j\beta_m z}}{4P_{mm}} \tilde{v}_{y_m}(x=0) \int_{-L/2}^{L/2} \left[T_y - \frac{1}{2} N_y \left(\frac{\omega^2 \rho}{C_{44}} - \beta_m^2 \right) \right] e^{j\beta_m z_0} dz_0 \\
&= \sum_m \tilde{u}_m(x) \frac{e^{-j\beta_m z}}{4P_{mm}} \tilde{v}_{y_m}(x=0) \int_{-L/2}^{L/2} \left[T_y - \frac{1}{2} \left(\frac{m}{h} \right)^2 N_y \right] e^{j\beta_m z_0} dz_0.
\end{aligned} \tag{28}$$

The modal amplitude for the problem of the tangential surface stress generated by an EMAT is finally given by:

$$A_m(z) = \frac{e^{-j\beta_m z}}{4P_{mm}} \tilde{v}_{y_m}(x=0) \int_{-L/2}^{L/2} \left[T_y - \frac{1}{2} \left(\frac{m}{h} \right)^2 N_y \right] e^{j\beta_m z_0} dz_0. \tag{29}$$

It is analytically related to EMAT characteristics through the moments of body forces, and also related to material characteristics, again through the moments but also through the propagation terms.

2.6. Brief summary of the theoretical model derived

The technical content of this section led to a semi-analytical solution for the modal amplitude of SH modes radiated by an EMAT into a ferromagnetic plate. To summarize, the first step consists in obtaining the magnetic field created by the specific wire configuration of the EMAT which writes as a Fourier series given by equation (7). The second step consists in calculating the body force generated by the EMAT which depends on the magnetic field; in the present configuration considered, the force to take into account is only the magnetostriction expressed by equation (12). In the third step, the zeroth and second order moments of this force are calculated by means of equation (A3). The fourth and final step consists in computing the convolution integral given by equation (29) to get the amplitude of the SH guided modes that exist at the working frequency considered. By Fourier synthesis, it is then possible to predict the transient field radiated by the EMAT.

In what follows, modal amplitudes for various EMATs are computed using the present model.

3. Two examples of application

3.1. Radiation by a meander-coil EMAT

A most studied EMAT is the so-called meander-coil. In this first example, the various calculation steps with intermediate results are shown. Current in the coil can be described as a function of z as shown by figure 2. This function is decomposed as a Fourier series given by:

$$S(z) = \sum_{n=0}^{\infty} \frac{4}{(2n+1)\pi} \cos\left(\frac{2(2n+1)\pi z}{D}\right) \sin\left(\frac{a(2n+1)\pi}{D}\right). \tag{30}$$

This EMAT is graphically described by figure 2.

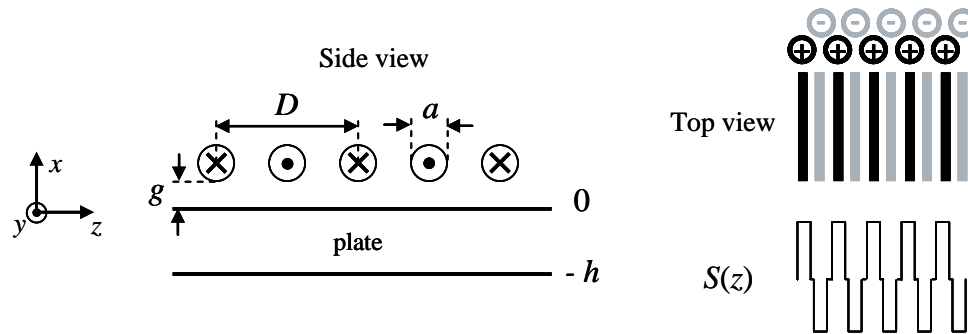


Figure 2. Left: Side view of a meander-coil EMAT. Right-top: Top view of the same EMAT. Right-bottom: a representation of the current passing through the coil.

In this example, the characteristics of the EMAT, of the material (iron) and the sampling in space and frequency are recorded in table 1: n is the number of wires, nS is the number of terms in the Fourier series, σ is the electrical conductivity and μ is the magnetic permeability of the material, n_z is the number of calculation points along the z -axis, n_x is the number of calculation points along the x -axis (the sampling is of 101 points for a depth of ten times the penetration depth δ , then of 10 points in the remaining thickness), $fmin$ is the first calculation frequency, $fmax$ the last, and finally, nf is the number of calculation frequencies.

Table 1. Characteristics of the EMAT, the material and the sampling in space and frequency.

n	17	-	ρ	7700	kg.m ⁻³	n_z	251	-
a	0.0005	m	h	0.003	m	n_x	101+10	-
D	0.002	m	μ_L	7.617 10 ¹⁰	Pa	$fmin$	0.1	MHz
nS	50	-	σ	9.93 10 ⁶	S.m ⁻¹	$fmax$	5	MHz
g	0.0001	m	μ	10000	-	nf	501	-

The magnetostrictive tensor $\bar{\bar{e}}$ [N.A⁻¹] is considered as not varying with the dynamic magnetic field. In our computations, we take:

$$\bar{\bar{e}}^t = \begin{bmatrix} - & - & - & 1.10^4 & - & 2.10^4 \\ - & - & - & - & - & - \\ - & - & - & 1.10^4 & - & 2.10^4 \end{bmatrix}. \quad (31)$$

Most of the values are not given because they are not involved in equation (15). A more detailed study of this tensor [7, 12] shows that most of these coefficients actually equal zero and that the others are expressed as functions of other material parameters. This has not been used here; it may describe better magnetostriction in particular circumstances. Figure 3 displays the current Fourier series $S(z)$.

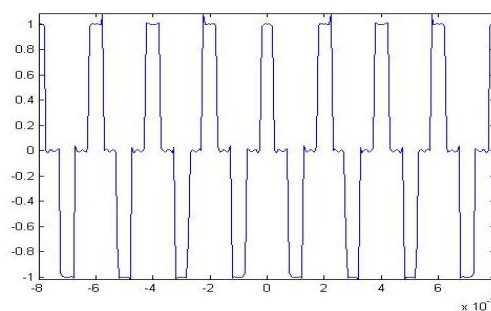


Figure 3. Current Fourier series $S(z)$ of a meander-coil.

It is a good approximation of the real current spatial distribution, with limited Gibbs phenomenon. The magnetic field created in the plate for an excitation frequency of 1 MHz is then calculated and shown by figure 4. The penetration depth effect is clearly visible: the field amplitude drastically decreases at very short distance of the surface. The body force is calculated and plotted on figure 5 (left). The corresponding surface stress is shown on figure 5 (right). Note that these plots display the absolute values of complex quantities. In practice, at a given frequency, the tangential surface stress acts on the plate surface with alternating positive and negative sign along the transducer length. Finally, the modal amplitude for different modes as a function of frequency are calculated and plotted on figure 6 (left). On figure 6 right, only the modal amplitude of the SH0 mode is plotted.

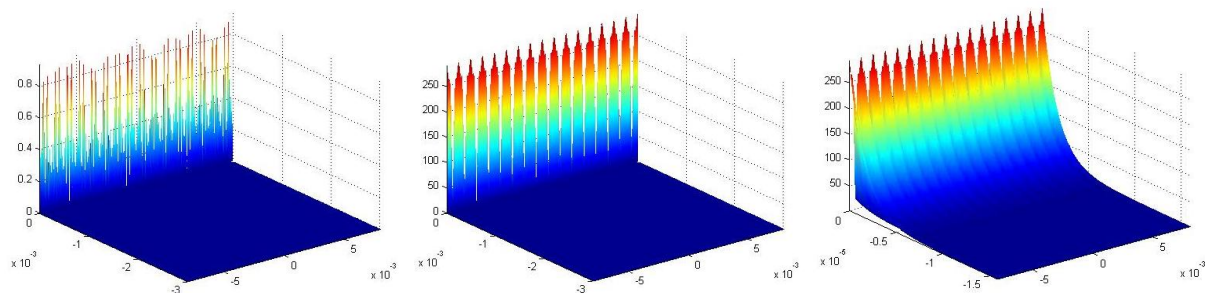


Figure 4. Magnetic field as a function of x (depth) and z (transducer length) created in an iron plate by a meander-coil EMAT at a frequency of 1 MHz. Left: x -component. Middle: z - component. Right: zoom on the z - component in the region near the top surface of the plate.

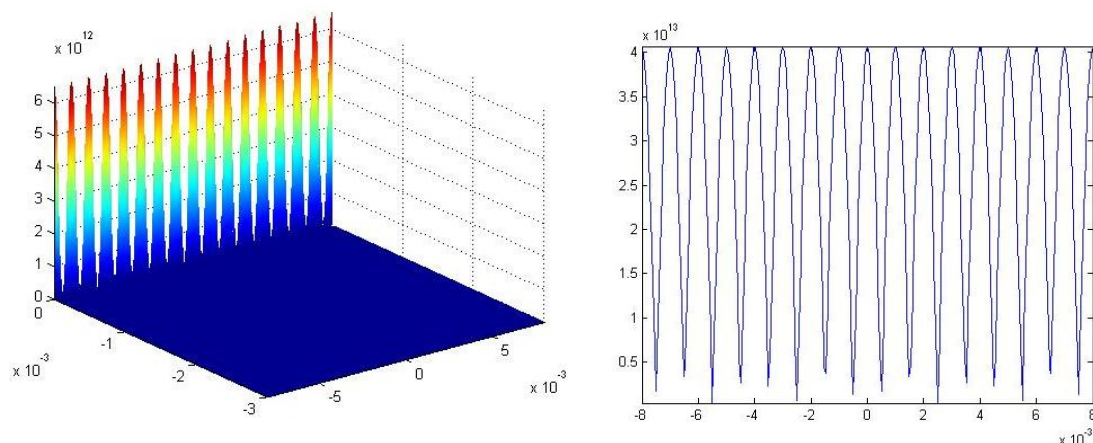


Figure 5. Body force (left) as a function of x (depth) and z (transducer length) and its equivalent surface stress (right) created by a meander-coil EMAT in an iron plate at 1 MHz. The equivalent surface stress is given for the SH0 mode only.

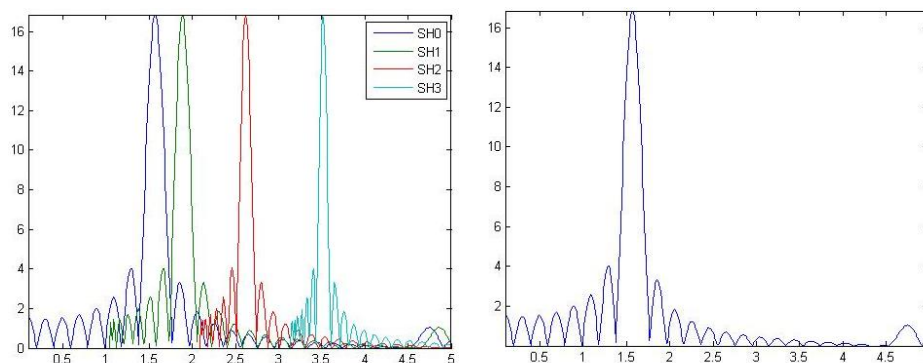


Figure 6. Left: modal amplitude over the frequency (in MHz) of the first four SH modes generated by the meander-coil. Right: same as left but only the SH0 mode is shown.

The modal amplitude variations with frequency for the different modes have a rather similar overall shape. The peak amplitudes are roughly equal and a resonance effect is clearly seen for all the modes considered. This last effect is due to the presence of the function *sinc* in the analytical expression of the modal amplitude typically of the form: $\text{sinc}(\beta_m - s_n)L/2$. When the spatial periodicity of the coil, represented by the term s_n , matches the wavelength β_m , the function *sinc* takes its maximal value. This arises at a frequency which differs from one mode to another.

3.2. Radiation by a uniform EMAT

A uniform EMAT is now considered as shown by figure 7.

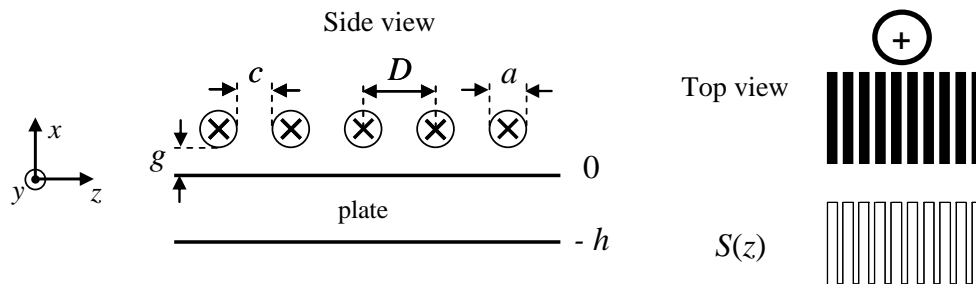


Figure 7. Left: Side view of a uniform EMAT. Right-top: Top view of the same EMAT. Right-bottom: a representation of the current passing through the wires.

In the following calculations, the two parameters a and c are equal. Other parameters (material etc.) are the same as those used for the meander-coil. On figure 8 are plotted modal amplitudes of the first four SH modes radiated for the uniform EMAT (left) from which is extracted that of the SH0 mode (right). A similar plot was presented for the meander-coil EMAT in figure 6.

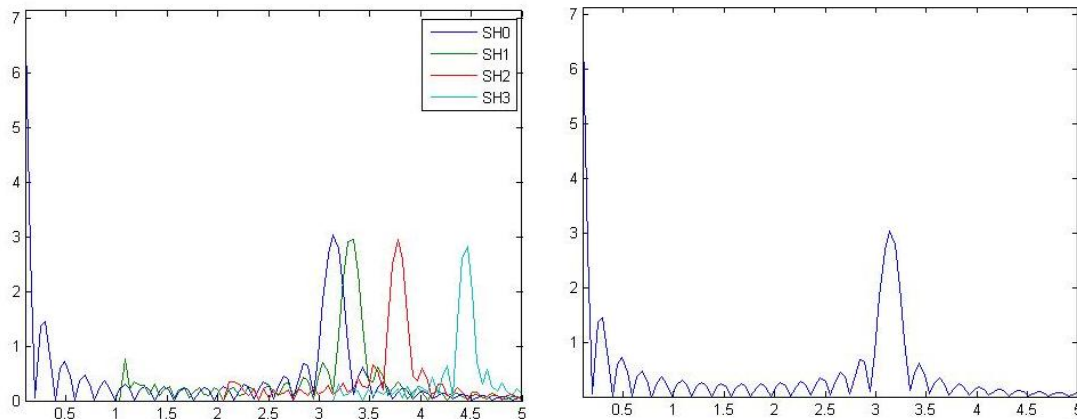


Figure 8. Left: modal amplitude over the frequency (in MHz) of the first four SH modes generated by the uniform EMAT, with $c=a$. Right: same as left but only the SH0 mode is shown.

This time, modal amplitudes vary with frequency from one mode to another. The first mode has its maximal value at null frequency; this continuous component was likely to appear with a uniform loading whereas it does not exist with spatially alternating loading of a meander-coil. Again, a modulation of amplitude is visible as for the meander-coil case; similarly, peak values correspond to a resonance when wire spacing coincides with the wavelength.

4. Conclusions

An analytical solution of the modal amplitude of SH guided modes generated by EMAT in a ferromagnetic plate has been developed. In the chain of sub-models developed for deriving the final formula, several offer more general capabilities to address other configurations than that of SH guided waves. In the present case, the formula developed allows fast and easy parametric studies if required

(such as those necessary for optimizing the design of a transducer). Experimental validations, extension to the 3D case and radiation of both surface and bulk waves will be further investigated.

5. Appendix. Transformation of body force into surface stress through a Taylor's series

The detailed derivation of the transformation of body force convolution integral into a surface stress convolution integral is complex and requires several steps of calculation. This calculation starts with the expression of the particle displacement as given by equation (14). Because the spatial variations of the Green's function are very low compared to those of body forces, the Green's function can be approximated by a Taylor series at the surface of the half-space. Here, the first three orders are taken into account:

$$G_{yy}(\vec{r}, \vec{r}_0) = G_{yy}(\vec{r}, \vec{r}_0|_{x_0=0}) + x_0 \frac{\partial G_{yy}(\vec{r}, \vec{r}_0|_{x_0=0})}{\partial x_0} + \frac{1}{2} x_0^2 \frac{\partial^2 G_{yy}(\vec{r}, \vec{r}_0|_{x_0=0})}{\partial x_0^2} + o(x_0^2) \quad (\text{A1})$$

To simplify notations, the point $\vec{r}_0|_{x_0=0}$ is denoted \vec{R}_0 in what follows. Substituting equation (A1) into equation (14) yields

$$u_y(\vec{r}) \approx \int_{-L/2}^{L/2} \left[G_{yy}(\vec{r}, \vec{R}_0) T_y(\vec{R}_0) + \frac{\partial G_{yy}(\vec{r}, \vec{R}_0)}{\partial x_0} M_y(\vec{R}_0) + \frac{1}{2} \frac{\partial^2 G_{yy}(\vec{r}, \vec{R}_0)}{\partial x_0^2} N_y(\vec{R}_0) \right] dz_0, \quad (\text{A2})$$

where T_y , M_y and N_y denote moments of the body force f_y , defined by:

$$T_y(\vec{R}_0) = \int_{-\infty}^0 f_y(\vec{r}_0) dx_0, \quad M_y(\vec{R}_0) = \int_{-\infty}^0 x_0 f_y(\vec{r}_0) dx_0 \quad \text{and} \quad N_y(\vec{R}_0) = \int_{-\infty}^0 x_0^2 f_y(\vec{r}_0) dx_0. \quad (\text{A3})$$

The following development aims at simplifying the derivative of the Green's function G_{yy} . This requires returning momentarily in 3D space. Using the definition of the strain tensor and the isotropy of the material, the local equilibrium Lamé's law is written as

$$\sum_j K_{ij}(\vec{r}_0) u_j(\vec{r}_0) = f_i(\vec{r}_0), \quad (\text{A4})$$

where $K_{ij}(\vec{r}_0) =$

$$\begin{pmatrix} -\omega^2 \rho - C_{11} \frac{\partial^2}{\partial x_0^2} - C_{44} \left(\frac{\partial^2}{\partial y_0^2} + \frac{\partial^2}{\partial z_0^2} \right) & -(C_{12} + C_{44}) \frac{\partial^2}{\partial x_0 \partial y_0} & -(C_{12} + C_{44}) \frac{\partial^2}{\partial x_0 \partial z_0} \\ -(C_{12} + C_{44}) \frac{\partial^2}{\partial x_0 \partial y_0} & -\omega^2 \rho - C_{11} \frac{\partial^2}{\partial y_0^2} - C_{44} \left(\frac{\partial^2}{\partial x_0^2} + \frac{\partial^2}{\partial z_0^2} \right) & -(C_{12} + C_{44}) \frac{\partial^2}{\partial y_0 \partial z_0} \\ -(C_{12} + C_{44}) \frac{\partial^2}{\partial x_0 \partial z_0} & -(C_{12} + C_{44}) \frac{\partial^2}{\partial y_0 \partial z_0} & -\omega^2 \rho - C_{11} \frac{\partial^2}{\partial z_0^2} - C_{44} \left(\frac{\partial^2}{\partial x_0^2} + \frac{\partial^2}{\partial y_0^2} \right) \end{pmatrix} \quad (\text{A5})$$

and where the components of the compliance matrix C are:

$$C_{12} = \lambda_L \quad ; \quad C_{44} = \mu_L \quad ; \quad C_{11} = C_{12} + 2C_{44} = \lambda_L + 2\mu_L. \quad (\text{A6})$$

The next steps will not solve the equations for the Green's function but develop some conditions that will help us to simplify equation (A2). By multiplying equation (A4) by G_{ki} , then, summing over i and finally integrating over the space, one gets:

$$\sum_{i,j} \int_{-\infty}^{+\infty} \int_{-\infty}^{+\infty} \int_{-\infty}^0 G_{ki}(\vec{r}, \vec{r}_0) K_{ij}(\vec{r}_0) u_j(\vec{r}_0) dy_0 dz_0 dx_0 = \sum_i \int_{-\infty}^{+\infty} \int_{-\infty}^{+\infty} \int_{-\infty}^0 G_{ki}(\vec{r}, \vec{r}_0) f_i(\vec{r}_0) dy_0 dz_0 dx_0. \quad (\text{A7})$$

Using the definition of the displacement as a spatial convolution between the Green's functions and the body forces, the displacement is now re-written as:

$$u_k(\vec{r}) = \sum_{i,j} \int_{-\infty}^{+\infty} \int_{-\infty}^{+\infty} \int_{-\infty}^0 G_{ki}(\vec{r}, \vec{r}_0) K_{ij}(\vec{r}_0) u_j(\vec{r}_0) dy_0 dz_0 dx_0. \quad (\text{A8})$$

Moreover, free boundary conditions are assumed on the surface of the half-space. Integrating by parts each term of the right-hand side of this last equation, using the boundary conditions and the fact that $\bar{\bar{G}}$ and \bar{u} tends to zero while the integration point tends to infinity, equation (A8) becomes

$$u_k(\vec{r}) = \sum_{i,j} \int_{-\infty}^{+\infty} \int_{-\infty}^{+\infty} \left[\int_{-\infty}^0 u_j(\vec{r}_0) K_{ij}(\vec{r}_0) G_{ki}(\vec{r}, \vec{r}_0) dx_0 + u_x(\vec{R}_0) \left[C_{11} \frac{\partial G_{kx}(\vec{r}, \vec{R}_0)}{\partial x_0} + C_{12} \left(\frac{\partial G_{ky}(\vec{r}, \vec{R}_0)}{\partial y_0} + \frac{\partial G_{kz}(\vec{r}, \vec{R}_0)}{\partial z_0} \right) \right] + u_y(\vec{R}_0) C_{44} \left[\frac{\partial G_{ky}(\vec{r}, \vec{R}_0)}{\partial x_0} + \frac{\partial G_{kx}(\vec{r}, \vec{R}_0)}{\partial y_0} \right] + u_z(\vec{R}_0) C_{44} \left[\frac{\partial G_{kx}(\vec{r}, \vec{R}_0)}{\partial z_0} + \frac{\partial G_{kz}(\vec{r}, \vec{R}_0)}{\partial x_0} \right] \right] dy_0 dz_0. \quad (\text{A9})$$

The conditions for the existence of $\bar{\bar{G}}$ are then:

$$\begin{aligned} \sum_i K_{ij}(\vec{r}_0) G_{ki}(\vec{r}, \vec{r}_0) &= \delta^3(\vec{r} - \vec{r}_0) \delta_{kj}, \\ C_{11} \frac{\partial G_{kx}(\vec{r}, \vec{R}_0)}{\partial x_0} + C_{12} \left(\frac{\partial G_{ky}(\vec{r}, \vec{R}_0)}{\partial y_0} + \frac{\partial G_{kz}(\vec{r}, \vec{R}_0)}{\partial z_0} \right) &= 0, \\ \frac{\partial G_{ky}(\vec{r}, \vec{R}_0)}{\partial x_0} + \frac{\partial G_{kx}(\vec{r}, \vec{R}_0)}{\partial y_0} &= 0 \quad \text{and} \quad \frac{\partial G_{kx}(\vec{r}, \vec{R}_0)}{\partial z_0} + \frac{\partial G_{kz}(\vec{r}, \vec{R}_0)}{\partial x_0} &= 0, \end{aligned} \quad (\text{A10})$$

where δ_{kj} is the Krönecker symbol.

Using equations (A10) and (A4), the conditions for $k = y$ are:

$$\begin{aligned} K_{xy}(\vec{r}_0) G_{yx}(\vec{r}, \vec{r}_0) + K_{yy}(\vec{r}_0) G_{yy}(\vec{r}, \vec{r}_0) + K_{zy}(\vec{r}_0) G_{yz}(\vec{r}, \vec{r}_0) &= -(C_{12} + C_{44}) \left(\frac{\partial^2 G_{yx}(\vec{r}, \vec{r}_0)}{\partial x_0 \partial y_0} + \frac{\partial^2 G_{yz}(\vec{r}, \vec{r}_0)}{\partial y_0 \partial z_0} \right) \\ &- \left[\omega^2 \rho + C_{11} \frac{\partial^2}{\partial y_0^2} + C_{44} \left(\frac{\partial^2}{\partial x_0^2} + \frac{\partial^2}{\partial z_0^2} \right) \right] G_{yy}(\vec{r}, \vec{r}_0) = 0, \end{aligned} \quad (\text{A11a})$$

$$C_{11} \frac{\partial G_{yx}(\vec{r}, \vec{R}_0)}{\partial x_0} + C_{12} \left(\frac{\partial G_{yy}(\vec{r}, \vec{R}_0)}{\partial y_0} + \frac{\partial G_{yz}(\vec{r}, \vec{R}_0)}{\partial z_0} \right) = 0, \quad (\text{A11b})$$

$$\frac{\partial G_{yy}(\vec{r}, \vec{R}_0)}{\partial x_0} + \frac{\partial G_{yx}(\vec{r}, \vec{R}_0)}{\partial y_0} = 0 \quad \text{and} \quad \frac{\partial G_{yx}(\vec{r}, \vec{R}_0)}{\partial z_0} + \frac{\partial G_{yz}(\vec{r}, \vec{R}_0)}{\partial x_0} = 0. \quad (\text{A11c and d})$$

Then, differentiating the second condition of equation (A11) with respect to y_0 leads to:

$$\frac{\partial^2 G_{yx}(\vec{r}, \vec{R}_0)}{\partial y_0 \partial x_0} = -\frac{C_{12}}{C_{11}} \left(\frac{\partial^2 G_{yy}(\vec{r}, \vec{R}_0)}{\partial^2 y_0} + \frac{\partial^2 G_{yz}(\vec{r}, \vec{R}_0)}{\partial y_0 \partial z_0} \right). \quad (\text{A12})$$

With the condition (A11a), the second derivative of G_{yy} with respect to x_0 is:

$$\begin{aligned} \frac{\partial^2 G_{yy}(\vec{r}, \vec{R}_0)}{\partial x_0^2} = & - \left[\frac{\omega^2 \rho}{C_{44}} + \frac{C_{11}^2 - C_{12}^2 - C_{12} C_{44}}{C_{11} C_{44}} \frac{\partial^2}{\partial y_0^2} + \frac{\partial^2}{\partial z_0^2} \right] G_{yy}(\vec{r}, \vec{R}_0) \\ & - \frac{(C_{12} + C_{44})(C_{11} - C_{12})}{C_{11} C_{44}} \frac{\partial^2 G_{yz}(\vec{r}, \vec{R}_0)}{\partial y_0 \partial z_0}. \end{aligned} \quad (\text{A13})$$

Finally, using the third condition (A11c), the first order derivative of G_{yy} with respect to x_0 is:

$$\frac{\partial G_{yy}(\vec{r}, \vec{R}_0)}{\partial x_0} = -\frac{\partial G_{yx}(\vec{r}, \vec{R}_0)}{\partial y_0}. \quad (\text{A14})$$

The first and the second derivatives of G_{yy} with respect to x_0 , given by equations (A14) and (A13), are substituted into equation (A2). Returning in 2D, derivatives with respect to y_0 vanish so that equation (A2) eventually becomes:

$$u_y(\vec{r}) \approx \int_{-L/2}^{L/2} \left[T_y - \frac{1}{2} N_y \left(\frac{\omega^2 \rho}{C_{44}} + \frac{\partial^2}{\partial z_0^2} \right) \right] G_{yy}(\vec{r}, \vec{R}_0) dz_0, \quad (\text{A15})$$

which corresponds to equation (16) in the body of the paper.

References

- [1] Hirao M and Ogi H 2003 *EMATS for Science and Industry: Noncontacting Ultrasonic Measurements* (Boston: Kluwer Academic Publishers)
- [2] Landau L and Lifshits E 2008 On the theory of the dispersion of magnetic permeability in ferromagnetic bodies *Ukr. J. Phys.* **53** 14-22 reprinted from 1935 *Phys. Zeitsch. der Sow.* **8** 153
- [3] Ahmadi B, Chazal H, Waeckerlé T and Roudet J 2010 *IEEE Trans. Magn.* **46** 4001
- [4] Ogi H 1997 *J. Appl. Phys.* **82** 3940
- [5] Thompson R B 1990 Physical principles of measurements with EMAT transducers *Physical Acoustics: Ultrasonic Measurement Methods* vol 19 chapter 4 pp 157–200
- [6] Auld B A 1973 *Acoustics fields and waves in solids* vol 2 (Malabar, Florida: Krieger publishing company)
- [7] Ogi H, Goda E and Hirao M 2003 *Jpn. J. Appl. Phys.* **42** 3020
- [8] Laguerre L, Aime J-C and Brissaud M 2002 *Ultrasonics* **39** 503
- [9] Hueter T F and Bolt R H *Sonics: Techniques for the Use of Sound and Ultrasound in Engineering and Science* (New York: John Wiley and Sons inc.)
- [10] Thompson R B 1980 *J. Nond. Eval.* **1** 79
- [11] Thompson R B 1973 *IEEE Trans. Son. Ultra.* **SU-20** 340
- [12] Ribichini R, Cegla F, Nagy P B and Cawley P 2010 *IEEE Trans. Ultra. Ferro. Freq. Cont.* **57** 2808